Improved Binding Free Energy Predictions from Single-Reference Thermodynamic Integration Augmented with Hamiltonian Replica Exchange

Ilja V. Khavrutskii* and Anders Wallqvist

Biotechnology HPC Software Applications Institute, Telemedicine and Advanced Technology Research Center, U.S. Army Medical Research and Materiel Command, Fort Detrick, Maryland 21702, United States

ABSTRACT: Reliable predictions of relative binding free energies are essential in drug discovery, where chemists modify promising compounds with the aim of increasing binding affinity. Conventional thermodynamic integration (TI) approaches can estimate corresponding changes in binding free energies but suffer from inadequate sampling due to the ruggedness of the molecular energy surfaces. Here, we present an improved TI strategy for computing relative binding free energies of congeneric ligands. This strategy employs a specific, unphysical single-reference (SR) state and Hamiltonian replica exchange (HREX) to locally enhance sampling. We then apply this strategy to compute relative binding free energies of 12 ligands in the L99A mutant of T4 lysozyme. Besides the ligands, our approach enhances hindered rotations of the important V111 as well as V87 and L118 side chains. Concurrently, we devise practical strategies to monitor and improve HREX-SRTI efficiency. Overall, the HREX-SRTI results agree well ($R^2 = 0.76$, RMSE = 0.3 kcal/mol) with available experimental data. When optimized for efficiency, the HREX-SRTI precision matches that of experimental measurements.

1. INTRODUCTION

High-quality predictions of binding free energies of small molecules to their biomolecular targets are important in drug design. The continued growth of computational power has enabled applications of statistical mechanics-based free energy perturbation (FEP) and thermodynamic integration (TI) methods to real life problems.[1−5] These advanced computational techniques are considered gold standards for binding free energy predictions, akin to isothermal titration calorimetry (ITC)—a technique that measures the binding free energies experimentally.[6,7]

Since their inception, great progress has been made in improving FEP and TI methods. Introduction of the soft-core potentials has made the calculations more reliable.[8−10] Subsequently, multiconfiguration simulation protocols[11] have laid the foundation for the application of generalized ensemble strategies such as Hamiltonian replica exchange (HREX)[12−17] which further improve the quality of the FEP and TI simulations.[18−22] Meanwhile, better postprocessing protocols have been developed that resulted in more reliable predictions of free energies and assessments of corresponding standard deviations.[4,23−27]

Despite this progress, binding free energy calculations remain challenging because of sampling limitations that are inherent in the molecular dynamics (MD) methods used in the simulations. Conventional FEP and TI free energy calculations are known to be sensitive to starting conformations of the bound complexes. For example, in a well-studied L99A mutant of T4 lysozyme, the conformation of the binding site residue V111 affects binding free energies of indene and p-xylene ligands by as much as 6 kcal/mol.[1,28−30] Other hindered residues can have a similar effect.[1] The predictions also depend on the initial orientation of the ligands in the binding pocket. These challenges are likely to be general and, therefore, need to be properly addressed.

Many enhanced sampling approaches have been devised to combat conformational challenges. It is impossible to list all of them here, but we will name a few that benefit alchemical free energy calculations. One of the earliest approaches scaled parts of the potential energy before and after an alchemical transformation to enhance sampling.[31] Recently, an approach called accelerated molecular dynamics (AMD) was combined with alchemical free energy calculations.[32−34] This approach adds a boosting potential to reduce barriers and is also independent of alchemical transformations.[35] Other methods exploited the alchemical transformations to enhance sampling. Examples include λ dynamics[36−38] or its Monte Carlo (MC) counterparts, such as chemical MC/MD[39,40] and more general simulated scaling.[41,42] In fact, these methods share important features with currently developing FEP and TI methods augmented with Hamiltonian replica exchange (HREX).[15−22,43]

Enhanced sampling will overcome dependence of FEP and TI predictions on the starting conformations and ultimately improve their accuracy and precision. Judiciously combining multiconfigurational FEP and TI methods with HREX can achieve enhanced sampling.[22,43] Previously, we presented a TI variant, called single-reference TI augmented with HREX (HREX-SRTI), which achieved convergence of solvation free energies for a challenging case of an amide system where conventional FEP and TI methods failed.[22] The amide in question had an internal barrier to cis/trans interconversion that was insurmountable in conventional MD simulations. HREX-SRTI was able to generate converged results using simulation times of only 4 ns.

In the present study, we apply HREX-SRTI to the well-studied T4 lysozyme mutant. Although this system has a simple binding

site—a hydrophobic cavity buried beneath the protein surface—it is sufficiently complex to render conventional FEP and TI approaches ineffective. Importantly, our binding free energy predictions for this system can be compared to the previously published independent computational and experimental values.[1,28−30]

First, we assess the variability in the free energy predictions using regular SRTI. Then, we employ SRTI with the HREX option and demonstrate that HREX efficiency is crucial to obtaining converged results. Thus, we provide practical recipes to improve the efficiency of HREX-SRTI simulations. Finally, we use one of these recipes to optimize HREX efficiency and obtain highly converged results for the most challenging of the ligands—indole.

2. METHODS

2.1. Parameters for Small Molecule Ligands. We studied 12 small molecules as follows: benzene, toluene, *o*-xylene, *p*-xylene, ethyl-benzene, *n*-propyl-benzene, *n*-butyl-benzene, *i*-butyl-benzene, phenol, indene, benzofuran, and indole. The initial coordinates of all of the small molecules in the present study were derived using the program CORINA.[44] Where applicable, we performed conformational expansion using the program ROTATE.[45] Two charge models described in sections 2.1.1 and 2.1.2 were used in combination with the GAFF force field for small molecules.[46] Each conformational ensemble was structurally refined through geometry optimization using the AM1 semiempirical quantum mechanical potential[47] as implemented in MOPAC7, version1.11.[48]

2.1.1. AM1BCC Charge Model. Partial charges from each unique conformation were accumulated using Boltzmann weighting with appropriate degeneracies by their AM1 energies at 300 K. The final AM1 charges were symmetrized where applicable and then augmented through the BCC procedure[49,50] implemented in the ANTECHAMBER program[51,52] from AMBER TOOLS, version 1.2. The resulting conformation-independent, properly symmetrized set of AM1BCC charges is expected to reproduce HF/6-31G(d) RESP charges to a good approximation.[53−56]

2.1.2. RESP Charge Model. For a select subset of molecules, we derived HF/6-31G(d) restricted electrostatic potential fit (RESP) partial charges using B3LYP/6-31G(d) optimized geometries. The geometry optimization and the electrostatic potential calculations were achieved using Gaussian 09.[57] The RESP fit[58] was performed using the ANTECHAMBER program.

2.2. Setup of Protein−Ligand Complexes. Coordinates of all of the ligands in complexes with the L99A mutant of T4 lysozyme were derived from a crystal structure (PDB: 181L) of the protein bound to benzene.[59] Initial placements of ligands other than benzene were derived using graph theory. Specifically, molecules were represented as graphs on the basis of their atom and bond types. Subsequently, association graphs were constructed, and maximal cliques were found to match atoms in the benzene rings of each molecule to those of the bound benzene.[60] There are 12 different cliques that give rise to 12 unique placements of each ligand within the binding site of the protein. Some of the cliques are degenerate depending on the symmetry of the molecule. Thus, for benzene, all 12 cliques are degenerate, yielding identical complex structures that differ only in the numbering of the carbon atoms of the ligand. However, for ligands such as benzofuran, indene, and indole, each clique yields a unique conformation of the complex.

By construction, initial protein coordinates and those of the benzene ring are identical for all of the complexes, while the
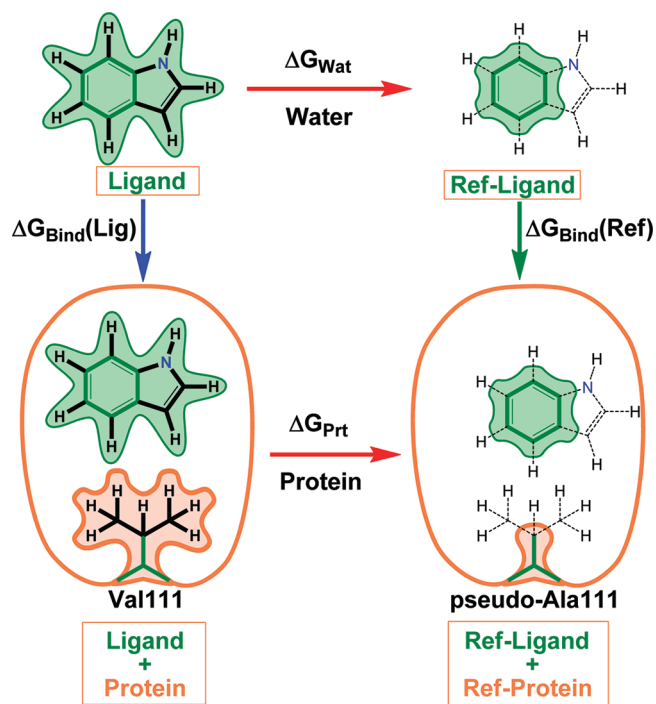

Figure 1. Thermodynamic cycle for computing binding free energies relative to an unhindered, unphysical reference state using SRTI. Horizontal arrows represent alchemical transformations of indole into the benzene core in water and the protein binding site. The protein residue V111 is alchemically converted to p-A at the same time. In the reference state, the molecular volumes of the ligand and the V111 residue (shown with green and brown shaded contours, respectively) are reduced due to disappearing atoms. The disappearing atoms interact with the rest of the system through soft-core Coulomb and vdW potentials and are connected to the reference core by dashed bonds. The torsional potentials associated with the virtual atoms are removed. These changes greatly enhance translational, rotational, and torsional degrees of freedom involved in the alchemical transformation with the help of HREX, thus activating rotation of the V111 and of the ligand in the binding site.

atoms protruding from the benzene ring change their position. In cases with branched ligands, such as *n*-propyl-, *n*-butyl-, and *i*-propyl-benzene, the protrusions have been examined for steric clashes with protein side chains.

The protein is described by an all-atom Amber 99SB molecular mechanics force field compatible with GAFF.[61] The solvation effects were modeled using a cubic periodic box of explicit TIP3P water molecules that extended at least 10 Å beyond the solute. The protein system was neutralized by adding nine $Cl^−$ ions.

2.3. Single Reference State. The choice of the reference states in SRTI determines which degrees of freedom of the system would be accelerated.[22] To allow for enhanced sampling of the ligands in the confines of the binding pocket, we chose the benzene core without hydrogen atoms as the reference state (Figure 1). Conveniently, our ligand reference state is independent of the charge model because the benzene core atoms have no charges by construction. Previously, we successfully employed this ligand reference state in computing free energies of hydration.[22]

Similarly, choosing an appropriate protein reference state could enhance sampling of the hindered protein side chains such as Val, Leu, Ile, and Thr. Each hindered residue could be mutated to a modified Ala residue referred to as pseudo-Ala (p-Ala).

Table 1. The L99A T4 Lysozyme Mutant Relative Binding Free Energies (Standard Deviations) to a Series of Benzene Derivatives[a]

compound	exptl	FEP	SRTI	Diff$_1$	HREX-SRTI	Diff$_2$	Wat%	Prt%
			AM1BCC Charge Model					
benzene	0.0(0.2)	0.0	0.0(0.3)	0.0	0.0(0.2)	0.0	34	29
phenol	2.5(N/A)	3.3	2.2(0.6)	−0.3	2.3(0.4)	−0.2	25	26
toluene	−0.3(0.2)	0.0	−0.1(0.3)	0.2	−0.2(0.2)	0.1	30	27
ethylbenzene	−0.6(0.2)	−1.8	−0.2(0.5)	0.3	−0.9(0.6)	−0.3	27	25
n-propylbenzene	−1.4(0.2)	−1.3	−0.4(0.5)	0.9	−1.5(0.4)	−0.2	26	23
n-butylbenzene	−1.5(0.2)	−0.3	−1.0(1.2)	0.5	−1.4(1.1)	0.1	23	21
i-butylbenzene	−1.3(0.2)	−0.5	−1.4(1.2)	−0.1	−1.3(0.7)	0.1	24	21
o-xylene	0.6(0.2)	3.3	1.0(0.4)	0.4	0.8(0.3)	0.2	28	25
p-xylene	0.5(0.2)	1.0	0.5(0.6)	0.0	0.4(0.3)	−0.1	29	26
indene	0.1(0.2)	2.8	1.3(0.4)	1.3	1.4(0.3)	1.3	21	20
indole	0.3(0.2)	4.1	2.9(1.7)	2.6	2.8(0.5)	2.5	14	21
benzofuran	−0.3(0.2)	1.0	0.4(0.5)	0.6	0.2(0.4)	0.5	24	22
RMS (cyclic)			(1.0)	1.7	(0.4)	1.7		
RMS (acyclic)			(0.7)	0.5	(0.5)	0.2		
RMS (all)			(0.8)	1.0	(0.5)	0.9		
			RESP Charge Model					
indene			−0.1(0.4)	−0.2	0.0(0.3)	−0.1	b	20
indole			0.6(1.9)	0.3	1.1(1.8)	0.8	b	19
benzofuran			−0.4(0.6)	−0.1	−0.8(0.4)	−0.5	b	22
RMS (cyclic)			(0.8)	0.2	(0.7)	0.5		
RMS (all)[c]			(1.1)	0.4	(1.1)	0.3		

[a] Energies are in kcal/mol relative to benzene. Averages and standard deviations are over eight (cyclic) or four (acyclic) independent simulations with distinct starting positions of the ligand in the binding site of the protein and two (all) independent simulations in water. Experimental and previously reported absolute binding free energies for benzene are −5.2 and −4.6 kcal/mol, respectively. [b] Because the effect of HREX on the simulations in water is small, regular simulations were performed. Diff$_1$ is the free energy difference between regular SRTI and experimental results; Diff$_2$ is the difference between HREX-SRTI and experimental results. The Wat and Prt columns contain acceptance ratios for the corresponding legs of the thermodynamic cycle (Figure 1). For these calculations, $p = 2$, and default values of $\alpha = 1.5$ parameters were used. Each simulation was run using 12 TI windows equally spaced in λ and 4-ns-long MD runs in the NPT ensemble at 1 atm and 300 K. The terms exptl and FEP represent previously published experimental and computational free energy perturbation benchmarks.[30] [c] Combined values with RESP@HF/6-31G(d) for cyclic and AM1BCC for acyclic compounds.

In p-Ala, hydrogen atoms of the methyl side chain are united with the Cβ carbon. A mutation of a hindered residue to p-Ala in the reference state would render its side chain atoms starting with Cβ virtual. Thus, HREX would enhance hindered rotations about bonds such as Cα−Cβ, Cβ−Cγ, and outward. In addition, the alchemical mutation of binding site residues to p-Ala can render the binding site in the reference state bigger, further aiding in the sampling of ligand transitions.

In this study, we simultaneously enhance sampling of the ligand and the protein side chains by combining the corresponding unphysical reference states.

2.4. TI Simulation Setup. In order to run the simulations, we employed GROMACS version 4.0.5 in single precision. Because the simulated system is described by Amber 99SB[61] and GAFF[46] molecular mechanical force fields that are not native to GROMACS, we used the PERL conversion script, which was described previously.[62] The script also automates setup of the alchemical transformation from the real to the reference state.

2.4.1. Soft-Core Potentials. In order to avoid the end-point catastrophe at the reference state, we employed soft-core electrostatic and LJ potentials[9,10] as implemented in GROMACS.[63−67] Earlier calculations employed a GROMOS style soft-core potential (eqs 1−3). Here, λ is the Hamiltonian coupling parameter, p is the coupling power, r is the distance between a given pair of atoms, α is the soft-core parameter, and σ is the radius of interaction computed from LJ parameters. For certain polar hydrogen atoms, σ is undefined, and in those cases a fixed value is used. Originally, we used $p = 2$, $\alpha = 1.5$, and $\sigma = 0.3$ as recommended in the user manual. Subsequently, to improve the acceptance ratio and level its distribution over TI window pairs, we used an alternative soft-core potential with $p = 1$.[10] For the latter potential, we reoptimized the value of α to arrive at $\alpha = 0.4$. The optimization of the α parameter was performed to achieve the best convergence behavior by monitoring standard deviations across independent TI runs. Other more complicated measures could be used to search for better alchemical paths, but these were not pursued in this study.[68]

$$V_{AB}^{sc}(r) = (1 - \lambda)\, V_A(R_A(r, \lambda)) + \lambda V_B(R_B(r, \lambda)) \qquad (1)$$

$$R_A(r, \lambda) = (\alpha \sigma_A^6 \lambda^p + r^6)^{1/6} \qquad (2)$$

$$R_B(r, \lambda) = (\alpha \sigma_B^6 (1 - \lambda)^p + r^6)^{1/6} \qquad (3)$$

2.4.2. MD Simulation Parameters. The production runs were performed in the NPT ensemble at $T = 300$ K and $P = 1$ atm, following the equilibration protocol described previously.[22]

The production run employed a Langevin thermostat and a Berendsen barostat,[64−67] with identical collision frequencies of $2\,ps^{-1}$.

Throughout the simulations, all of the bonds containing hydrogen atoms were constrained using LINCS,[69] and the integration time step was set to 2 fs. We employed the particle mesh Ewald (PME) approach for electrostatics[64−67] with a 1 nm real space cutoff and switched off van der Waals interactions over the range of 0.8−0.9 nm. Typically, production runs were 2-ns-long for each TI window, but in some cases they were extended to 4 ns. The coordinates of the system were recorded every 1000 steps for subsequent analyses.

2.4.3. Regular SRTI Simulations. To obtain the alchemical free energies or reversible works, the real and reference states of each system corresponded to values 0 and 1 of the Hamiltonian coupling parameter λ, respectively. Each alchemical SRTI transformation employed M equally separated λ windows. The majority of the simulations used $M = 12$, but in some cases simulations were performed with $M = 23$. All λ windows of an SRTI simulation had the same initial configuration. For each λ window, we recorded $\partial V/\partial \lambda$ values at every time step. The mean values $\langle \partial V/\partial \lambda \rangle$ for all of the λ windows were assembled into the final work using the Fourier beads integration procedure, which was described previously.[22]

Averages of the final work values and their standard deviations were computed using several independent simulations. Specifically, for proteins in complex with cyclic molecules (benzofuran, indene, and indole), we performed eight simulations each with distinct starting positions of the ligand. For acyclic (not cyclic) molecules, we only performed four such simulations. Finally, for all of the ligands in water, we performed two independent simulations. The differences between the alchemical work values in water and protein environments yielded the relative binding free energies with respect to the unphysical reference state. The final relative binding free energies and their standard deviations were reported with respect to benzene.

2.4.4. HREX-SRTI Simulations. In order to run HREX-SRTI simulations, we employed an in-house PERL script interfaced with GROMACS. Replica exchanges were attempted every 1000 MD steps or 2 ps. For the majority of the simulations, we attempted exchanges a total of 2000 times resulting in 4-ns-long simulations of each window. In special cases, the number of exchange attempts was reduced to 1000, decreasing the simulation time to 2 ns per window. Following the exchanges, each λ window received a new random seed to restart its MD run. All of the other simulation details were the same as those associated with regular SRTI simulations.

2.4.5. Analysis of SRTI and HREX-SRTI Results. The analysis of real state trajectories was performed with standard GROMACS tools. Specifically, the g_angle program was used to obtain time series of dihedral angles of the hindered side chains. For the Val side chain, we gathered data on the Hα−Cα−Cβ−Hβ (κ_1) dihedral, and for the Leu side chain, data on Hα−Cα−Cβ−Cγ (κ_1) and Cα−Cβ−Cγ−Hγ (κ_2) dihedrals were collected. For HREX-SRTI simulations, the real state trajectory had to be assembled from short trajectories using an in-house PERL script that followed the state through all of the exchanges.

3. RESULTS AND DISCUSSION

In order to demonstrate the utility of the SRTI approach in computing relative binding free energies, we studied ligand binding to a well-defined binding site in the L99A mutant of T4 lysozyme. Specifically, we chose a congeneric series of 12 ligands derived from benzene that has been studied previously.[28−30] We distinguished two classes of compounds within the series according to their structure outside the common benzene motif, namely cyclic and acyclic. Thus, benzofuran, indene, and indole were considered cyclic, whereas all of the remaining compounds were considered acyclic. Because all of the ligands in the series (Table 1), with the exception of benzene, can have multiple orientations in the binding pocket, this system presents a considerable challenge for binding free energy calculations.

The cyclic and acyclic ligands behave differently when in complex with the protein. For acyclic ligands, the benzene ring can flip without an overall structural change to the complex. For cyclic ligands, the benzene flip alters the overall structure of the complex. Hence, for cyclic ligands, i.e., benzofuran, indene, and indole, we selected eight orientations (four for each of the two states resulting from the benzene flip). The degeneracy with respect to the benzene flip allowed us to reduce the number of representative orientations to four for the remaining acyclic ligands. Thus, for each ligand, we performed simulations with different initial orientations in the binding pocket.

The conformations of the active site residues are equally important and should be considered when determining binding free energies.[28−30] For the L99A mutant of T4 lysozyme, the conformational state of the V111 side chain profoundly affects the computed binding free energies. Because this residue lines the surface of the binding site, inadequate sampling of its conformations has been shown to cause discrepancies of as much as 6 kcal/mol.[28−30] Other residues in the active site may have similar effects on binding free energies.[1] Hence, we need to improve sampling of the ligand and relevant protein conformations at the same time. This combination makes the problem particularly challenging.

3.1. Regular SRTI Simulations. *3.1.1. AM1BCC Charge Model.* The average variability in the relative binding free energies from regular SRTI is 0.7 kcal/mol (Table 1). Most of the ligands have standard deviations in the range of 0.3−0.6 kcal/mol. However, the largest acyclic ligands, *n*-butyl-benzene and *i*-butyl-benzene, show increased standard deviations of 1.2 kcal/mol. Surprisingly, one of the cyclic ligands, indole, exhibits a record high standard deviation of 1.7 kcal/mol. Indole, like other cyclic ligands, is expected to have hindered flip transitions in the binding site.

In comparison to experimental values, the regular SRTI approach has an RMSE of 1.0 kcal/mol relative to and excluding benzene. Smaller ligands are in good agreement—within 0.3 kcal/mol—with the available experimental data (Table 1). It should be noted that only an upper estimate of binding free energy is available for phenol, which does not bind the T4 lysozyme mutant well. For more extended acyclic molecules, such as *n*-propyl- and *n*-butyl-benzenes, the agreement is not as favorable, with *n*-propyl-benzene demonstrating the highest deviation of 0.9 kcal/mol. The predicted binding free energy for *i*-butyl-benzene is serendipitously within 0.1 kcal/mol of the experimental value. Interestingly, the cyclic ligands exhibit the largest deviations of all compounds, diverging by as much as 2.6 kcal/mol in the case of indole.

The disagreement between computed and experimental binding free energies for the heterocyclic compounds is instructive. In particular, the results for indene and benzofuran ligands were well-converged judging by the low standard deviations (Table 1). In contrast, the binding free energy of indole exhibited a large standard deviation of 1.7 kcal/mol. These observations suggest that issues other than sampling could be responsible for the
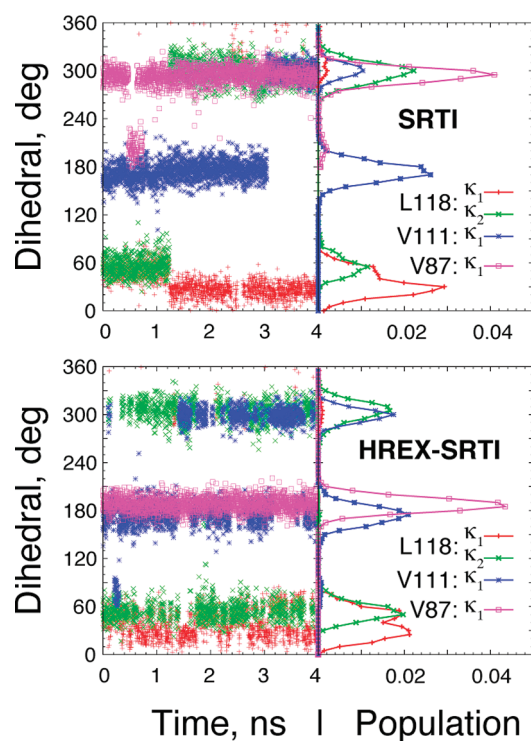
Figure 2. Side chain conformational transitions for the indole complex with the L99A mutant of T4 lysozyme using the V87p-A:V111p-A: L118p-A reference. Time series and respective histograms are presented for the κ_1 (Hα−Cα−Cβ−Hβ) torsion of V111 and V87 and for the κ_1 (Hα−Cα−Cβ−Cγ) and κ_2 (Cα−Cβ−Cγ−Hγ) torsions of L118. The bins of the histograms were 5° wide. The time series reports the corresponding values of the torsions. The top panel summarizes the regular SRTI simulation results with relatively few conformational transitions, whereas the bottom panel shows the HREX-SRTI results with numerous such transitions. The reported HREX-SRTI simulations employed 12 windows and the optimized $p = 1$ soft cores.

Figure 3. Side chain conformational transitions for indole complex with the L99A mutant of T4 lysozyme using the V111p-A reference. Time series and respective histograms are presented for the κ_1 (Hα−Cα−Cβ−Hβ) torsion of V111. The bins of the histograms were 5° wide. The time series report the corresponding values of the torsions. The top panel summarizes the regular SRTI simulation results with relatively few conformational transitions, whereas the bottom panel displays the HREX-SRTI results with numerous such transitions. The reported HREX-SRTI simulations employed 12 windows and the optimized $p = 1$ soft cores.

overall disagreement with experimental results. Because we employed the AM1BCC charge model, which approximates the RESP HF/6-31G(d) partial charges, we decided to assess the effect of the model.

3.1.2. RESP Charge Model for Cyclic Compounds. Using RESP HF/6-31G(d) charges for the cyclic compounds considerably improved the agreement of regular SRTI predictions with experimental values. Indeed, while simulations with the AM1BCC charge model systematically overestimated the binding free energies, with the RESP charges the disagreement was no longer systematic and remained within 0.3 kcal/mol. Thus, for indole, the RESP charges lowered the disagreement with experimental values by more than 2 kcal/mol. Despite the improved accuracy of the predictions, the RESP charges did not affect convergence of the cyclic ligands. Indole still had the largest standard deviation of 1.9 kcal/mol. These results suggest that a charge model can strongly affect the accuracy, but not necessarily the precision, of the computed binding free energies.

Large standard deviations in computed binding free energies identify ligands most sensitive to the initial complex configuration. The reasons for this sensitivity likely reside in hindered ligand motions. Indeed, inspecting trajectories of the ground state simulations for benzofuran using all 12 starting configurations, we found that they converge to only four
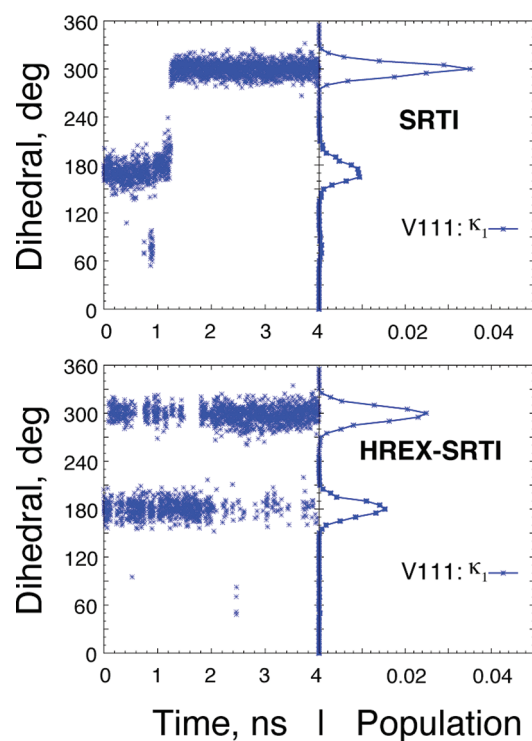
metastable configurations. These metastable configurations demonstrate that the cyclic ligands do not flip freely in the binding pocket on a nanosecond time scale. Furthermore, alignment of the ligands suggests that the binding pocket has the geometry of a flattened prolate ellipsoid. Each unique configuration contributes distinctly to the binding free energy, thus, increasing the standard deviation. Therefore, enhanced sampling of the ligands in their complexes would allow the metastable configurations to rapidly interconvert, ultimately improving the quality of predictions. Because the regular SRTI approach does not have the ability to enhance these transitions alone, we need to invoke the HREX option.

3.2. Improving the SRTI Results with HREX. The use of SRTI with HREX[22] could simultaneously enhance sampling of the ligand and select protein side chains. First, we attempted to enhance motions of the ligand and the V111 side chain. Specifically, by choosing the benzene core as a ligand reference state, we intended to activate rotations of the bulkier ligands within the active site. Furthermore, by choosing a V111p-A mutant as a protein reference state (see the Methods section for definition), we expected to activate the V111 rotations that have activation barriers in the 5−8 kcal/mol range.[29,70] This strategy is expected to reduce the size of each ligand to the size of the benzene core while simultaneously enlarging the binding site around p-A111 (Figure 1) to

Table 2. Improving HREX-SRTI Efficiency for the L99A T4 Lysozyme Mutant in Complex with Indole[a]

system	N_{SRTI}	p	α	ΔG_{Prt}(SD), kcal/mol	N_{HREX}	accept, %
			V87p-A:V111p-A:L118p-A			
SRTI	*12*	*2*	*1.5*	*34.2(3.8)*		
SRTI	*23*	*2*	*1.5*	*36.9(3.3)*		
HREX-SRTI	23	2	1.5	39.5(1.4)	1000[b]	30
HREX-SRTI	12	1	0.3	29.4(0.9)	2000	17
HREX-SRTI	12	1	0.4	30.6(0.8)	2000	13
HREX-SRTI	12	1	0.5	33.6(1.2)	2000	9
			V111p-A			
SRTI	*12*	*2*	*1.5*	*−0.6(1.8)*		
HREX-SRTI	12	2	1.5	−1.0(1.8)	2000	19
HREX-SRTI	23	2	1.5	−1.6(0.5)	2000	48
HREX-SRTI	12	1	0.4	−1.7(0.2)	2000	29

[a] These results are representative of the protein leg of the thermodynamic cycle (Figure 1) using RESP@HF/6-31G(d) point charges on the ligand. N_{SRTI} and N_{HREX} refer to the number of TI windows and exchange cycles, respectively. Soft-core parameters involved in optimization are p and α (see text for description). Averages and standard deviations (SD) are over eight independent simulations with distinct starting positions of the ligand in the binding site. Two unphysical references, namely, V87p-A:V111p-A:L118p-A and V111p-A, are considered. By design, the use of the former reference with HREX should enhance side chain torsions of the V87, V111, and L118 along with rotation and flipping of the ligand. The latter reference should enhance torsions of the V111 side chain and rotations of the ligand. Unless otherwise stated, all TI windows were run in the NPT ensemble at 1 atm and 300 K for 4 ns. [b] Each window was run for 2 ns.

activate ligand flip transitions which are important in the evaluation of cyclic compounds.

Interestingly, regular SRTI simulations suggest that the V111 rotation does not significantly affect relative free energies of many ligands in the series. The free energy barrier for the valine rotation is such that it could spontaneously rotate on a time scale of several nanoseconds.[29,70] Indeed, we observed that during 4-ns-long unenhanced SRTI simulations of the ground state, V111 does spontaneously flip a few times without having a significant effect on the binding free energies of many molecules in the series (Figures 2 and 3, top panels).

The absence of the previously reported effect of V111[28−30] in cases of *p*-xylene and indene, among other ligands, is not surprising. It could be explained by the fact that SRTI computes relative binding free energies as opposed to the absolute free energies reported previously. Indeed, in the present SRTI setup, we do not need to sample an empty binding site of the protein, where V111 has a preferred conformation.[29] Nevertheless, for the largest acyclic ligands, the effect could still be significant. Therefore, we expect that enhancing the rotation of the V111 side chain through HREX would improve the overall agreement with experimental data. This approach can also be applied to enhance V111 rotation in the absolute binding free energy calculations with TI.

3.2.1. AM1BCC Charge Model and HREX-SRTI. Simply turning on the HREX option in SRTI with the V111p-A reference state produced seemingly modest improvements over the corresponding regular SRTI results (Table 1). The average standard deviation for all of the ligands decreased from 0.7 to 0.5 kcal/mol with the AM1BCC charge model. However, some of the

ligands enjoyed significantly lower standard deviations versus regular SRTI. For example, *i*-butyl-benzene and indole, which had among the highest standard deviations, experienced significant drops from 1.2 to 0.7 kcal/mol and from 1.7 to 0.5 kcal/mol, respectively.

For the AM1BCC model, the overall agreement with experimental values improved only slightly, with RMSE decreasing to 0.9 kcal/mol. Most of the improvement was achieved for the acyclic ligands, which, when separated from the rest of the ligands, showed a change in RMSE from 0.5 to 0.2 kcal/mol. The cyclic compounds with AM1BCC charges are unaffected by HREX and persistently show an RMSE of 1.7 kcal/mol. Despite the improved agreement with experimental data, larger acyclic ligands still exhibit elevated standard deviations, particularly in the case of *n*-butyl-benzene.

The lack of significant improvements could indicate that other residues in the binding site might be important. Most notably, all of these simulations used 12 windows and consequently had modest acceptance ratios (Table 1). Indole in water had the lowest acceptance ratio of 14%, which increased to 21% in the protein environment with the V111p-A reference. Indole and phenol are the only two ligands in the series that have polar hydrogen atoms and an increased acceptance ratio in the protein environment.

3.2.2. RESP Charge Model and HREX-SRTI. Different charge models behave distinctly when running SRTI with the HREX option. Thus, HREX-SRTI with RESP charges for the cyclic compounds diminished the agreement with experimental results compared with that in regular SRTI. Specifically, RMSE for the three cyclic compounds increased from 0.2 to 0.5 kcal/mol. However, the average standard deviations decreased from 0.9 to 0.8 kcal/mol (Table 1). Unexpectedly, indole exhibited a sharply increased standard deviation of 1.8 kcal/mol using the RESP model compared to 0.5 kcal/mol with the AM1BCC model.

3.3. Improving HREX-SRTI Predictions. To understand the reason for poor convergence of the free energy values with HREX-SRTI and to possibly improve the results, we examined the indole system in greater detail. Specifically, we focused on the indole simulations with RESP charges that exhibited the largest disagreement with experimental values and the largest standard deviation.

3.3.1. Triple Mutant Reference State V87p-A:V111p-A:L118p-A. We hypothesized that even with the HREX option turned on, flipping of the indole might still be impeded in the V111p-A reference state. In order to test this hypothesis, we created a triple mutant reference state by mutating two additional residues, V87 and L118 to p-A. These two residues pin the benzene moiety of the ligands to the floor of the binding site. It should be noted that L118 has been experimentally shown to exhibit conformational variability similarly to V111.[1]

The triple mutant system V87p-A:V111p-A:L118p-A should completely remove the ligand flipping restriction. Moreover, this unphysical reference state could potentially open water access to the hydrophobic binding site of the L99A T4 lysozyme. In the proposed experiment, three residues would undergo alchemical transformations, making 30 atoms of the protein (nine for each valine and 12 for leucine) disappear in the reference state. While this should theoretically enhance sampling of the three residues along with the ligand, it might be difficult in practice to achieve a sufficient overall exchange rate in HREX-SRTI.[22] Hence, this test would also identify the limits of our approach in extending it to concurrent activation of multiple residues.

The triple mutant V87p-A:V111p-A:L118p-A presents a challenge for HREX-SRTI. As seen in Table 2, regular SRTI simulations with 12 and 23 windows had standard deviations of 3.8 and 3.3 kcal/mol, respectively, for just the protein leg of the thermodynamic cycle (Figure 1). The fact that the standard deviation with the triple mutant reference is more than twice as large as that with the single mutant one (1.8 kcal/mol) suggests that conformations of residues V87 and L118 may indeed affect ligand binding. The standard deviation was reduced to 1.4 kcal/mol when employing 23 windows in the HREX-SRTI simulations. The corresponding 12-window simulations did not achieve a sufficient overall exchange rate to yield results that were distinct from the regular SRTI simulations.

3.3.2. Assessing HREX Efficiency. 3.3.2.1. Round-Trip Count. Achieving efficient exchanges is critical for obtaining converged free energies in HREX simulations.[43] The overall acceptance ratio might be inadequate to assess the efficiency of HREX simulations. While the overall acceptance ratio is a satisfactory criterion to assess the efficiency of the more widely applied temperature replica exchange (TREX) simulations in the absence of first order transitions,[71,72] the situation with HREX is different.

It is difficult to devise a universal exchange protocol for HREX simulations, because the Hamiltonian generally depends on λ nonlinearly.[15,16] One way to monitor the efficiency of HREX simulations is to examine the number of round-trips made over the simulation time.[42,71] A replica that has returned to its initial λ after visiting both $\lambda = 0$ and $\lambda = 1$ states in either order is said to have accomplished a round-trip. Although this is an excellent measure of efficiency in theory, simulations might not, in practice, be long enough to complete even a single round-trip. In addition, when increasing a number of windows, a round-trip may take longer time. Therefore, long simulation times may be required to use this measure of exchange efficiency.

Finally, we note that besides the $\lambda = 1$ window in SRTI, scaling of the dihedral and soft-core potentials can activate hindered transitions in several neighboring windows. This means that multiple windows can experience enhanced sampling. While a standard round-trip count would reflect the overall efficiency of the simulations, it may not capture diffusion of the conformations from all of the enhanced windows down to the $\lambda = 0$ window. Ultimately, we gauge the sampling gains by the reduction in the standard deviations of HREX-SRTI compared to regular SRTI, which is an independent measure of both convergence and sampling efficiency.

3.3.2.2. Acceptance Ratio Profile. Alternatively, one can generate an acceptance ratio profile for each pair of TI windows that is adjacent in λ space from the actual simulation data.[15] A flat profile would indicate equally probable exchanges between adjacent windows and, consequently, produce the largest number of round-trips possible for any given time. Therefore, we consider the acceptance ratio profile a practical alternative to the round-trip count. A simple inspection of the acceptance ratio profile could identify problems in the HREX simulations. The pair with the lowest ratio across all of the window pairs limits the round-trip rate.

3.3.2.3. Energy Difference Histograms. The acceptance ratio profile is related to the corresponding double and single energy difference histograms. Single energy difference histograms over all adjacent pairs of λ_i and λ_{i+1} involve the corresponding forward and backward energy differences. These histograms contain valuable information not only with respect to the efficiency of the simulations but also with respect to their validity.[73] Furthermore, the information from the forward and backward histograms can be used to estimate the free energy difference between the adjacent
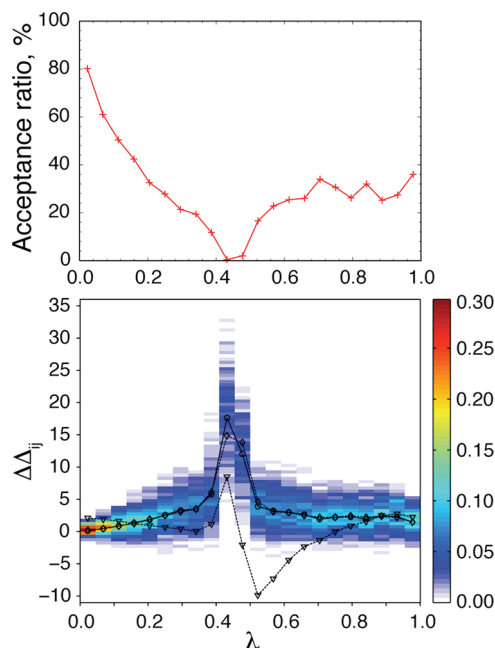

Figure 4. Monitoring efficiency of HREX-SRTI. The top panel illustrates the acceptance ratio profile for indole bound to the L99A mutant of T4 lysozyme with the V87p-A:V111p-A:L118p-A reference state. The bottom panel shows the $\Delta\Delta_{ij}$ histograms in color. On the top of the histograms is the actual profile of the mean $\Delta\Delta_{ij}$ value (solid black line with circles), its estimate from the variance (dashed black line with diamonds), and the contribution of the derivative of the $\langle\partial V/\partial\lambda\rangle$ (dashed black line with triangles), which are derived from eq 4. The HREX-SRTI simulations employed 23 windows, each run for 2 ns with $p = 2$ soft-core potentials in the NPT ensemble at 1 atm and 300 K.

states, though such an estimator may be suboptimal.[43,73] In cases with linear dependence of the Hamiltonian on λ, the single energy difference histogram is closely related to the corresponding histogram of the energy derivative with respect to λ.[43] The double energy difference histogram comprises the energy change of the generalized ensemble that enters the Metropolis function to decide on the exchange of a particular pair.[15] These double energy difference histograms are perhaps the most informative for the purpose of the HREX. They could be computed using configurations generated by regular SRTI for a given set of λ values at an additional expense that would increase the cost of the calculation to that of HREX-SRTI.

3.3.3. Parameters That Influence HREX Efficiency. Predicting the dependence of the double energy difference or the acceptance ratio profile on the coupling parameter λ without actually running HREX simulations could help design more efficient simulations. Indeed, determining an optimal set of λ values that would yield a uniform acceptance ratio profile will maximize the efficiency. It is easy to show that the mean of the double energy difference histograms and the $\langle\partial V/\partial\lambda\rangle$ are related according to eq 4 (see the Appendix for derivation):

$$\langle\Delta\Delta_{ij}\rangle \approx \beta(\Delta\lambda_{ij})^2\left(\left\langle\frac{\partial^2 V}{\partial\lambda^2}\right\rangle_{(\lambda_i+\lambda_j)/2} - \frac{d}{d\lambda}\left\langle\frac{\partial V}{\partial\lambda}\right\rangle_{(\lambda_i+\lambda_j)/2}\right)$$

$$\approx \beta^2(\Delta\lambda_{ij})^2\mathrm{var}\left(\frac{\partial V}{\partial\lambda}\right)_{(\lambda_i+\lambda_j)/2} \tag{4}$$

Figure 4 shows an overlay of the $\Delta\Delta_{ij}$ distributions, their actual mean value, and its approximation using eq 4. As can be seen from Figure 4, eq 4 closely approximates the mean of the double energy difference. Furthermore, the contribution of the mean second derivative is significant and should not be neglected. Thus, eq 4 is a useful starting point for improving HREX simulation protocols.

It might be worthwhile to note that the derivative in the latter equation is related to the variance of the $\partial V/\partial\lambda$:[43,74]

$$\mathrm{var}\left\langle\frac{\partial V}{\partial\lambda}\right\rangle = \left\langle\left(\frac{\partial V}{\partial\lambda}\right)^2\right\rangle - \left\langle\frac{\partial V}{\partial\lambda}\right\rangle^2 = \beta^{-1}\left(\left\langle\frac{\partial^2 V}{\partial\lambda^2}\right\rangle - \frac{d}{d\lambda}\left\langle\frac{\partial V}{\partial\lambda}\right\rangle\right)$$

(5)

According to eq 5, in cases when the potential V depends on λ linearly, the variance reduces to the first derivative of the $<\partial V/\partial\lambda>$. Because the variance is a positive quantity, the left-hand side of eq 4 would always be positive. Assuming that the value of the mean double energy difference would correspond to the most probable value of its distribution, one might expect better acceptance ratios if the mean is closer to zero. For nonlinear dependence, convexity of the potential with respect to λ would play an important role.

3.3.3.1. Increasing the Number of TI Windows. Equation 4 suggests that reducing the spacing between adjacent λ's (increasing the number of windows) would result in an increase in the acceptance probability. Indeed, similarly to our previous study,[22] increasing the number of windows from 12 to 23 in the system with the V87-pA:V111-pA:L118-pA reference state considerably improves the overall acceptance ratio from less than 10% to 30%. The reduction in standard deviation from 3.3 to 1.4 kcal/mol attests to the improved efficiency. It should be noted that the cost of the 23-window HREX-SRTI simulations was maintained similar to that of the 12-window simulation by reducing the number of exchange cycles to 1000.

The acceptance ratio profile of the HREX-SRTI simulations with V87-pA:V111-pA:L118-pA reference and 23 windows (shown in Figure 4) revealed an exchange bottleneck. Indeed, as seen in Figure 4, the acceptance ratio for the pair of windows with $\lambda_i = 0.4091$ and $\lambda_{i+1} = 0.4545$ is close to zero. In other words, our generalized ensemble was divided, with replicas sampling two independent regions of the λ space. This prevented the system from reaching a true equilibrium. Clearly, the 23-window HREX simulations, while greatly improving the overall acceptance ratio, still had the limitation of inefficient exchanges in a specific region of the λ space.

3.3.3.2. Position of Windows. Although generally applicable, simply increasing the number of windows to improve the efficiency of HREX simulations is not a viable strategy. Certainly, if successive TI windows were kept at constant λ intervals, this strategy would not remove the existing exchange bottlenecks. In addition, maintaining the number of windows at the same level as in regular SRTI simulations would be desirable from a computational cost perspective. Therefore, a better strategy would be to adjust the positions of the existing TI windows. Importantly, regular TI is sufficient for obtaining the $\partial V/\partial\lambda$ variance profile that according to eq 4 could be used to determine an optimal set of λ's for efficient HREX simulations. Alternatively, round-trip-based methods could be used to optimize placement of λ's as has been done in the context of simulated
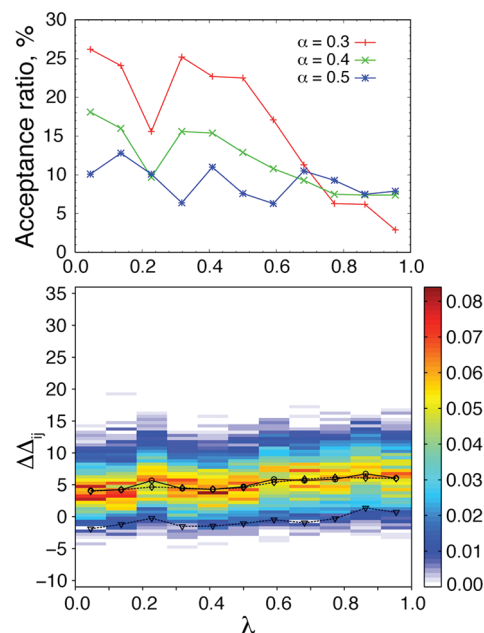

Figure 5. Optimization of HREX-SRTI efficiency by altering soft-core potential parameters. The top panel illustrates the acceptance ratio profiles for indole bound to the L99A mutant of T4 lysozyme with the V111p-A reference state. Unlike in Figure 4, these simulations employed $p = 1$ soft-core potentials with three different values for the parameter α, namely 0.3, 0.4, and 0.5. The bottom panel shows the $\Delta\Delta_{ij}$ histograms in color along with their actual mean (solid black line with circles), the estimate of the mean from the $\partial V/\partial\lambda$ variance (dashed black line with diamonds), and the contribution of the derivative of the $<\partial V/\partial\lambda>$ (dashed black line with triangles), which are derived from eq 4. The bottom panel only shows results for the simulations with $\alpha = 0.4$ that achieve the best precision. The HREX-SRTI simulations employed only 12 windows, each run for 4 ns in the NPT ensemble at 1 atm and 300 K.

scaling.[42] However, determining the optimal set of λ's is highly system-dependent. Therefore, we did not pursue this strategy here. Fortunately, eq 4 suggests yet another strategy for improving HREX-SRTI simulations.

3.3.3.3. Altering Mean Force Profile. Besides manipulating the number and position of TI windows, eq 4 indicates that the acceptance probability is greatly affected by the shape of the $\partial V/\partial\lambda$ variance profile. Therefore, we could improve the exchange rates by changing the shape of the profile using parameters we have at our disposal. Specifically, we can vary parameters of the soft-core potentials.

Recall the general form of the soft-core potentials available in GROMACS[9,10,63,75] (eqs 1−3). The present implementation of GROMACS supports soft-cores with $p = 1$ and $p = 2$.[9,10] The α and σ parameters have been optimized for each p using an approach that decouples Coulomb and vdW changes.[76] For the SRTI approach that simultaneously transforms Coulomb and vdW interactions, these values of parameters may be suboptimal.

Soft-core potentials with $p = 1$ are well-suited for HREX-SRTI simulations. Indeed, our earlier SRTI simulations with $p = 2$ potentials had the limitation of sharp peaks in the $\langle\partial V/\partial\lambda\rangle$ profile near $\lambda = 0$ as previously described in the literature.[9,67] These peaks are due to the hydrogen atoms with undefined σ parameters and present an obstacle to accurate integration within the Fourier beads approach.[22] In order to integrate these sharp peaks
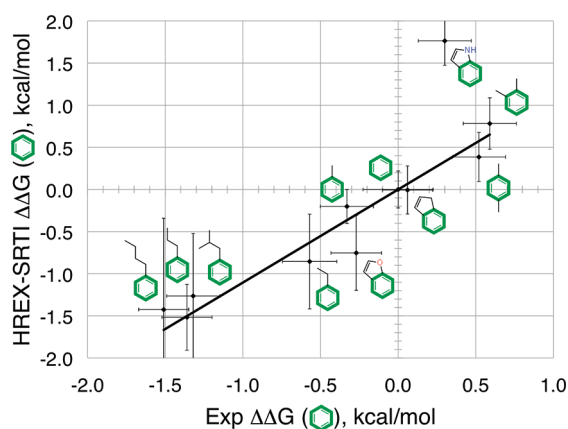
Figure 6. Comparison of the HREX-SRTI relative binding free energy predictions to experimental results. The binding free energies are relative to benzene. The best-fitted line passing through the origin is $y = 1.10x$, and the corresponding correlation coefficient is $R^2 = 0.76$. The RESP HF/6-31G(d) charge model was used for the cyclic compounds, and the AM1BCC model was used for the acyclic compounds. With the exception of indole, all of the simulations employed $p = 2$ soft-cores with default parameters. The indole prediction incorporates the results obtained with the optimized $p = 1$ soft-cores.

properly, additional TI windows have been introduced. In contrast, the profile derived using $p = 1$ soft-core potentials is devoid of such peaks.[10]

Switching to the soft-core potentials with $p = 1$ improves the acceptance ratio of the HREX-SRTI simulations. Indeed, using default parameters with only 12 windows, we obtained modest acceptance ratios of 17% in the system that had the V87-pA:V111-pA:L118-pA reference. Recall that 12-window simulations with $p = 2$ failed to achieve acceptance ratios above 10%. However, as discussed above, an improved acceptance ratio does not guarantee improved efficiency. The analysis of the acceptance ratio profile for $p = 1$ shows that windows near $\lambda = 1$ exchange poorly.

3.3.3.4. Optimization of Soft-Core Parameters for HREX. The optimization of the α parameter helps to flatten the acceptance ratio profile, rendering the HREX-SRTI more efficient. Using 12-window simulations of indole with the V87-pA:V111-pA:L118-pA reference, we varied the value of α from its default value of 0.3 to 0.4 and 0.5 at $p = 1$. Figure 5 summarizes the acceptance ratio profiles and compares predicted and actual mean $\Delta\Delta_{ij}$ for the best of them. While at α = 0.5 we obtained the most uniform acceptance ratio profile, the overall acceptance ratio declined to 9% (Table 2). At the intermediate value of 0.4, the overall acceptance ratio was 13%, with the acceptance ratio profile demonstrating sufficient exchange probabilities near $\lambda = 1$. Clearly, one has to find a compromise between the flatness of the acceptance ratio profile and the overall acceptance ratio.

To choose the best value of parameter α, we compared the standard deviations from each set of simulations. As seen in Table 2, the intermediate value α = 0.4 yielded the lowest standard deviations of 0.8 kcal/mol. This is a considerable improvement for the system with the triple mutant reference, in comparison to the regular 12-window SRTI simulation with $p = 2$, which had a standard deviation of 3.8 kcal/mol. Interestingly, simulations with α = 0.5 that were associated with an almost flat acceptance ratio profile yielded a standard deviation of 1.2 kcal/mol.

3.3.3.5. Transferability of Optimized Parameters. The value of α optimized for the challenging system with the V87-pA:V111-pA:L118-pA reference state could be transferred to improve the results for an easier system with the V111-pA reference. With the latter reference state, only the V111 side chain is enhanced along with the ligand in HREX-SRTI. Indeed, as seen in Table 2, for $p = 2$, the HREX-SRTI simulations with 12 windows and the V111-pA reference achieved a standard deviation of 1.8 kcal/mol. In fact, HREX-SRTI and regular SRTI had identical standard deviations, despite the fact that the overall acceptance ratio of the former was 19%. With 23 windows, both the acceptance ratio and the standard deviation improved to 48% and 0.5 kcal/mol, respectively. To our great satisfaction, the optimized HREX-SRTI with $p = 1$ demonstrated significantly improved convergence. Remarkably, we were able to achieve an improved standard deviation of 0.2 kcal/mol using only 12 windows with an overall acceptance ratio of 29%.

Even with the optimized protocol, our predictions for indole deviate significantly from the experimental data. Figure 6 shows the comparison of our predicted binding free energies with the experimental values for all of the ligands, including the optimized results for indole. Indeed, the binding free energy of indole using the most efficient HREX-SRTI protocol is still overestimated by 1.5 kcal/mol.

3.3.3.6. Decoupling of Coulomb and vdW Transformations. As a final note on efficiency, we would like to mention that the $\langle \partial V/\partial \lambda \rangle$ profile would change radically by decoupling of the vdW and Coulomb transformations. Such a decoupling is expected to render the overall profile smoother and hence improve the acceptance ratio.[21] Indeed, HREX simulations with decoupled vdW and Coulomb transformations were recently reported.[20,21] Unfortunately, the overall acceptance ratios or acceptance ratio profiles were not provided. Since the HREX-SRTI approach was originally designed[22] to electrostatically guide ligands to better binding poses,[77,78] decoupling of the electrostatics and vdW would defeat the purpose.

3.4. HREX-SRTI As a Conformational Analysis Tool. It is instructive to analyze structural transitions in the L99A T4 lysozyme mutant in complex with indole in an attempt to explain the observed disagreement with experimental values.

3.4.1. Transitions of Hindered Residues Are Indeed Enhanced by HREX-SRTI. In order to demonstrate that HREX-SRTI enhances conformational transitions of the hindered protein side chains, we performed additional analyses of the real state trajectories ($\lambda = 0$). Figures 2 and 3 compare the dihedral angles, described in the Methods section, that characterize side chain conformations of V87, V111, and L118 where applicable. Although the histograms of the referred to dihedral angles may look similar, the time series clearly demonstrate the increased number of transitions in HREX-SRTI. In most cases, each side chain samples multiple conformational basins, supporting our earlier conclusion regarding their contributions to the binding free energies. Interestingly, the V87 side chain appears to consistently prefer a particular conformation.

3.4.2. Indole Transitions in the Binding Pocket. We also verified that indole could flip its benzene plane in HREX-SRTI simulations with triple mutant reference states. The analysis of the real state trajectories revealed multiple indole orientations in the binding pocket. In one of the orientations, the NH group of indole persistently hydrogen-bonded with the S atom of M102. In another orientation, the same NH group was involved in hydrogen bonding with the backbone carbonyl group of V87.

In the HREX-SRTI simulations with the single mutant V111p-A reference state, the ligand in-plane rotation was enhanced, but the plane flipping transitions remained hindered.

3.4.3. Water Does Not Bind T4 Lysozyme Mutant with Indole. The indole disagreement with experimental values is not attributable to a lack of water access to the binding site. Although our simulations with the V111p-A reference state are not designed to open the normally sealed active site, we have tested this hypothesis using the V87p-A:V111p-A:L118p-A reference state. By inspecting the MD trajectories, we observed that water molecules did penetrate the pocket of the triple mutant reference state ($\lambda = 1$). However, none of the configurations with water molecules inside the binding site reached the real state ($\lambda = 0$) during the HREX-SRTI simulations. This strongly suggests that water is not responsible for the observed discrepancy.

4. CONCLUSIONS

This study presented a practical application of the SRTI approach to compute relative binding free energies of small molecules to a challenging binding site in the L99A mutant of T4 lysozyme. With the HREX option, SRTI successfully enhanced sampling of the hindered transitions of protein side chains and bound ligands. Achieving efficient HREX simulations improves the quality of predictions. However, the commonly used overall acceptance ratio is not a good indicator of the efficiency of the HREX. Instead, acceptance ratio profiles should be examined and whenever possible made uniform by adjusting simulation parameters. To aid the future design of efficient simulation protocols, we have provided a useful relationship between the mean exchange energy and the corresponding $\partial V/\partial \lambda$ variance profiles. Guided by the relationship, we demonstrated that judicial changes in the soft-core potentials considerably improved HREX-SRTI simulation efficiency. Overall, the HREX-SRTI predicted relative binding free energies for a series of 12 ligands with an RMSE of 0.3 kcal/mol comparable to experimental data. Ultimately, improving efficiency of the HREX simulations may further reduce computational cost and increase the precision of the predictions.

Note, while this paper was under revision, we discovered a paper by Steiner and coauthors that used an approach identical to HREX-SRTI to compute relative free energies of a number of ligands to Plasmepsin II, albeit without accelerating any residues of the protein.[79]

■ APPENDIX

For a configuration R, the vertical excitation energy $\Delta_{ij}(R)$ from a Hamiltonian at λ_i to that at λ_j is calculated as follows:

$$\Delta V_{ij}(R) = V(R, \lambda_j) - V(R, \lambda_i) \tag{A1}$$

The overall potential energy change $\Delta\Delta_{ij}(R,R')$ for the generalized ensemble upon Hamiltonian exchange between two configurations R and R' from the adjacent windows λ_i and λ_j is

$$\Delta\Delta_{ij}(R, R') = \beta[\Delta V_{ij}(R)]_{\lambda_i} + \beta[\Delta V_{ji}(R')]_{\lambda_j} \tag{A2}$$

The subscripts after the square brackets indicate the Hamiltonian of the simulations used to obtain the respective configurations. Only two configurations representing each λ are involved.

The generalized ensemble average value of the double difference for a given pair of adjacent replicas is then

$$\langle\Delta\Delta_{ij}\rangle = \beta\langle\Delta V_{ij}\rangle_{\lambda_i} + \beta\langle\Delta V_{ji}\rangle_{\lambda_j} \tag{A3}$$

Using second order Taylor expansion:

$$[\Delta V_{ij}(R)]_{\lambda_i} \approx \left[\frac{\partial V(R)}{\partial \lambda}\right]_{\lambda_i} \Delta\lambda_{ij} + \frac{1}{2}\left[\frac{\partial^2 V(R)}{\partial \lambda^2}\right]_{\lambda_i}(\Delta\lambda_{ij})^2 \tag{A4}$$

where

$$\Delta\lambda_{ij} = \lambda_j - \lambda_i \tag{A5}$$

we obtain the following expression, which is equivalent to eq 4 in the main text:

$$\langle\Delta\Delta_{ij}\rangle \approx \beta\Delta\lambda_{ij}\left(\left\langle\frac{\partial V}{\partial \lambda}\right\rangle_{\lambda_i} - \left\langle\frac{\partial V}{\partial \lambda}\right\rangle_{\lambda_j}\right)$$
$$+ \frac{\beta(\Delta\lambda_{ij})^2}{2}\left(\left\langle\frac{\partial^2 V}{\partial \lambda^2}\right\rangle_{\lambda_i} + \left\langle\frac{\partial^2 V}{\partial \lambda^2}\right\rangle_{\lambda_i}\right)$$
$$\approx \beta(\Delta\lambda_{ij})^2\left(\left\langle\frac{\partial^2 V}{\partial \lambda^2}\right\rangle_{\lambda_{(i+j)/2}} - \frac{d}{d\lambda}\left\langle\frac{\partial V}{\partial \lambda}\right\rangle_{\lambda_{(i+j)/2}}\right) \tag{A6}$$

Recalling eq 5 from the main text we obtain the final relation.

$$\langle\Delta\Delta_{ij}\rangle \approx \beta^2(\Delta\lambda_{ij})^2\,\text{var}\left\langle\frac{\partial V}{\partial \lambda}\right\rangle_{\lambda_{(i+j)/2}} \tag{A7}$$

■ AUTHOR INFORMATION

Corresponding Author
*E-mail: ikhavrutskii@bioanalysis.org.

■ REFERENCES

(1) Boyce, S. E.; Mobley, D. L.; Rocklin, G. J.; Graves, A. P.; Dill, K. A. *J. Mol. Biol.* **2009**, *394*, 747.

(2) Gallicchio, E.; Levy, R. M. *Curr. Opin. Struct. Biol.* **2011**, *21*, 161.

(3) Aleksandrov, A.; Thompson, D.; Simonson, T. *J. Mol. Recognit.* **2010**, *23*, 117.

(4) Bruckner, S.; Boresch, S. *J. Comput. Chem.* **2011**, *32*, 1303.

(5) Chodera, J. D.; Mobley, D. L.; Shirts, M. R.; Dixon, R. W.; Branson, K.; Pande, V. S. *Curr. Opin. Struct. Biol.* **2011**, *21*, 150.

(6) Leavitt, S.; Freire, E. *Curr. Opin. Struct. Biol.* **2001**, *11*, 560.

(7) Chaires, J. B. *Annu. Rev. Biophys.* **2008**, *37*, 135.

(8) Straatsma, T. P.; McCammon, J. A. *J. Chem. Phys.* **1994**, *101*, 5032.

3010

dx.doi.org/10.1021/ct2003786 |*J. Chem. Theory Comput.* 2011, 7, 3001–3011

(9) Beutler, T. C.; Mark, A. E.; van Schaik, R. C.; Gerber, P. R.; van Gunsteren, W. F. *Chem. Phys. Lett.* **1994**, *222*, 529.

(10) Shirts, M. R.; Pande, V. S. *J. Chem. Phys.* **2005**, *122*, 134508.

(11) Straatsma, T. P.; McCammon, J. A. *J. Chem. Phys.* **1991**, *95*, 1175.

(12) Kwak, W.; Hansmann, U. H. E. *Phys. Rev. Lett.* **2005**, *95*, 138102.

(13) Fukunishi, H.; Watanabe, O.; Takada, S. *J. Chem. Phys.* **2002**, *116*, 9058.

(14) Sugita, Y.; Kitao, A.; Okamoto, Y. *J. Chem. Phys.* **2000**, *113*, 6042.

(15) Hritz, J.; Oostenbrink, C. *J. Chem. Phys.* **2007**, *127*, 204104.

(16) Hritz, J.; Oostenbrink, C. *J. Chem. Phys.* **2008**, *128*, 144121.

(17) Hritz, J.; Oostenbrink, C. *J. Phys. Chem. B* **2009**, *113*, 12711.

(18) Woods, C. J.; Essex, J. W.; King, M. A. *J. Phys. Chem. B* **2003**, *107*, 13703.

(19) Woods, C. J.; King, M. A.; Essex, J. W. *Lect. Notes Comput. Sci. Eng.* **2006**, *49*, 251.

(20) Jiang, W.; Hodoscek, M.; Roux, B. *J. Chem. Theory Comput.* **2009**, *5*, 2583.

(21) Jiang, W.; Roux, B. *J. Chem. Theory Comput.* **2010**, *6*, 2559.

(22) Khavrutskii, I. V.; Wallqvist, A. *J. Chem. Theory Comput.* **2010**, *6*, 3427.

(23) Shirts, M. R.; Pande, V. S. *J. Chem. Phys.* **2005**, *122*, 144107.

(24) Shirts, M. R.; Chodera, J. D. *J. Chem. Phys.* **2008**, *129*, 124105.

(25) Shirts, M. R.; Bair, E.; Hooker, G.; Pande, V. S. *Phys. Rev. Lett.* **2003**, *91*, 140601.

(26) Bennett, C. H. *J. Comput. Phys.* **1976**, *22*, 245.

(27) Kumar, S.; Bouzida, D.; Swendsen, R. H.; Kollman, P. A.; Rosenberg, J. M. *J. Comput. Chem.* **1992**, *13*, 1011.

(28) Deng, Y.; Roux, B. *J. Chem. Theory Comput.* **2006**, *2*, 1255.

(29) Mobley, D. L.; Chodera, J. D.; Dill, K. A. *J. Chem. Theory Comput.* **2007**, *3*, 1231.

(30) Mobley, D. L.; Graves, A. P.; Chodera, J. D.; McReynolds, A. C.; Shoichet, B. K.; Dill, K. A. *J. Mol. Biol.* **2007**, *371*, 1118.

(31) Mark, A. E.; van Gunsteren, W. F.; Berendsen, H. J. C. *J. Chem. Phys.* **1991**, *94*, 3808.

(32) Wereszczynski, J.; McCammon, J. A. *J. Chem. Theory Comput.* **2011**, *6*, 3285.

(33) Fajer, M.; Hamelberg, D.; McCammon, J. A. *J. Chem. Theory Comput.* **2008**, *4*, 1565.

(34) Fajer, M.; Swift, R. V.; McCammon, J. A. *J. Comput. Chem.* **2009**, *30*, 1719.

(35) Hamelberg, D.; Mongan, J.; McCammon, J. A. *J. Chem. Phys.* **2004**, *120*, 11919.

(36) Kong, X. J.; Brooks, C. L. *J. Chem. Phys.* **1996**, *105*, 2414.

(37) Banba, S.; Guo, Z.; Brooks, C. L. *J. Phys. Chem. B* **2000**, *104*, 6903.

(38) Bitetti-Putzer, R.; Yang, W.; Karplus, M. *Chem. Phys. Lett.* **2003**, *377*, 633.

(39) Eriksson, M. A. L.; Pitera, J.; Kollman, P. A. *J. Med. Chem.* **1999**, *42*, 868.

(40) Pitera, J.; Kollman, P. *J. Am. Chem. Soc.* **1998**, *120*, 7557.

(41) Li, H.; Fajer, M.; Yang, W. *J. Chem. Phys.* **2007**, *126*, 024106.

(42) Zheng, L.; Yang, W. *J. Chem. Phys.* **2008**, *129*, 124107.

(43) Min, D.; Li, H.; Li, G.; Bitetti-Putzer, R.; Yang, W. *J. Chem. Phys.* **2007**, *126*, 144109.

(44) Sadowski, J.; Gasteiger, J.; Klebe, G. *J. Chem. Inf. Comput. Sci.* **1994**, *34*, 1000.

(45) Renner, S.; Schwab, C. H.; Gasteiger, J.; Schneider, G. *J. Chem. Inf. Model.* **2006**, *46*, 2324.

(46) Wang, J.; Wolf, R. M.; Caldwell, J. W.; Kollman, P. A.; Case, D. A. *J. Comput. Chem.* **2004**, *25*, 1157.

(47) Dewar, M. J. S.; Zoebisch, E. G.; Healy, E. F.; Stewart, J. J. P. *J. Am. Chem. Soc.* **1985**, *107*, 3902.

(48) Stewart, J. J. P. *MOPAC7*; University of Texas, Austin: Austin, TX.

(49) Jakalian, A.; Bush, B. L.; Jack, D. B.; Bayly, C. I. *J. Comput. Chem.* **2000**, *21*, 132.

(50) Jakalian, A.; Jack, D. B.; Bayly, C. I. *J. Comput. Chem.* **2002**, *23*, 1623.

(51) Wang, J. *Antechamber* **2009**, *1*, 2.

(52) Wang, J.; Wang, W.; Kollman, P. A.; Case, D. A. *J. Mol. Graphics Model.* **2006**, *25*, 247.

(53) Nicholls, A.; Mobley, D. L.; Guthrie, J. P.; Chodera, J. D.; Bayly, C. I.; Cooper, M. D.; Pande, V. S. *J. Med. Chem.* **2008**, *51*, 769.

(54) Mobley, D. L.; Bayly, C. I.; Cooper, M. D.; Dill, K. A. *J. Phys. Chem. B* **2009**, *113*, 4533.

(55) Mobley, D. L.; Bayly, C. I.; Cooper, M. D.; Shirts, M. R.; Dill, K. A. *J. Chem. Theory. Comput.* **2009**, *5*, 350.

(56) Shivakumar, D.; Deng, Y.; Roux, B. *J. Chem. Theory Comput.* **2009**, *5*, 919.

(57) Frisch, M. J.; Trucks, G. W.; Schlegel, H. B.; Scuseria, G. E.; Robb, M. A.; Cheeseman, J. R.; Scalmani, G.; Barone, V.; Mennucci, B.; Petersson, G. A.; Nakatsuji, H.; Caricato, M.; Li, X.; Hratchian, H. P.; Izmaylov, A. F.; Bloino, J.; Zheng, G.; Sonnenberg, J. L.; Hada, M.; Ehara, M.; Toyota, K.; Fukuda, R.; Hasegawa, J.; Ishida, M.; Nakajima, T.; Honda, Y.; Kitao, O.; Nakai, H.; Vreven, T.; Montgomery, J. A., Jr.; Peralta, J. E.; Ogliaro, F.; Bearpark, M.; Heyd, J. J.; Brothers, E.; Kudin, K. N.; Staroverov, V. N.; Kobayashi, R.; Normand, J.; Raghavachari, K.; Rendell, A.; Burant, J. C.; Iyengar, S. S.; Tomasi, J.; Cossi, M.; Rega, N.; Millam, N. J.; Klene, M.; Knox, J. E.; Cross, J. B.; Bakken, V.; Adamo, C.; Jaramillo, J.; Gomperts, R.; Stratmann, R. E.; Yazyev, O.; Austin, A. J.; Cammi, R.; Pomelli, C.; Ochterski, J. W.; Martin, R. L.; Morokuma, K.; Zakrzewski, V. G.; Voth, G. A.; Salvador, P.; Dannenberg, J. J.; Dapprich, S.; Daniels, A. D.; Farkas, Ö.; Foresman, J. B.; Ortiz, J. V.; Cioslowski, J.; Fox, D. J. *Gaussian 09*, Revision A.1; Wallingford, CT, 2009.

(58) Bayly, C. I.; Cieplak, P.; Cornell, W.; Kollman, P. A. *J. Phys. Chem.* **1993**, *97*, 10269.

(59) Morton, A.; Matthews, B. W. *Biochemistry* **1995**, *34*, 8576.

(60) Bron, C.; Kerbosch, J. *Commun. ACM* **1973**, *16*, 575.

(61) Hornak, V.; Abel, R.; Okur, A.; Strockbine, B.; Roitberg, A.; Simmerling, C. *Proteins* **2006**, *65*, 712.

(62) Mobley, D. L.; Chodera, J. D.; Dill, K. A. *J. Chem. Phys.* **2006**, *125*, 084902.

(63) Van Der Spoel, D.; Lindahl, E.; Hess, B.; Groenhof, G.; Mark, A. E.; Berendsen, H. J. *J. Comput. Chem.* **2005**, *26*, 1701.

(64) Berendsen, H. J. C.; van der Spoel, D.; van, D. R. *Comput. Phys. Commun.* **1995**, *91*, 43.

(65) Hess, B.; Kutzner, C.; van der Spoel, D.; Lindahl, E. *J. Chem. Theory Comput.* **2008**, *4*, 435.

(66) Van Der Spoel, D.; Lindahl, E.; Hess, B.; Groenhof, G.; Mark, A. E.; Berendsen, H. J. C. *J. Comput. Chem.* **2005**, *26*, 1701.

(67) van der Spoel, D.; Lindahl, E.; Hess, B.; Kutzner, C.; van Buuren, A. R.; Apol, E.; Meulenhoff, P. J.; Tieleman, D. P.; Sijbers, A. L. T. M.; Feenstra, K. A.; Drunen, R. v.; Berendsen, H. J. C. *GROMACS User Manual Version 4.0*; The GROMACS development team: Groningen, The Netherlands, 2006.

(68) Blondel, A. *J. Comput. Chem.* **2004**, *25*, 985.

(69) Hess, B.; Bekker, H.; Berendsen, H. J. C.; Fraaije, J. G. E. M. *J. Comput. Chem.* **1997**, *18*, 1463.

(70) Khavrutskii, I. V.; Fajer, M.; McCammon, J. A. *J. Chem. Theory Comput.* **2008**, *4*, 1541.

(71) Trebst, S.; Troyer, M.; Hansmann, U. H. E. *J. Chem. Phys.* **2006**, *124*, 174903.

(72) Yeh, I.-C.; Lee, M. S.; Olson, M. A. *J. Phys. Chem. B* **2008**, *112*, 15064.

(73) Pohorille, A.; Jarzynski, C.; Chipot, C. *J. Phys. Chem. B* **2010**, *114*, 10235.

(74) Simonson, T. *Mol. Phys.* **1993**, *80*, 441.

(75) Lange, O. F.; Schaefer, L. V.; Grubmueller, H. *J. Comput. Chem.* **2006**, *27*, 1693.

(76) Bash, P. A.; Singh, U. C.; Langridge, R.; Kollman, P. A. *Science* **1987**, *236*, 564.

(77) Sines, J. J.; Allison, S. A.; McCammon, J. A. *Biochemistry* **1990**, *29*, 9403.

(78) Tan, R. C.; Truong, T. N.; McCammon, J. A.; Sussman, J. L. *Biochemistry* **1993**, *32*, 401.

(79) Steiner, D.; Oostenbrink, C.; Diederich, F.; Zurcher, M.; van Gunsteren, W. F. *J. Comput. Chem.* **2011**, *32*, 1801.